The Impact of Cation Intercalation on the Electronic Structure of $Ti_3C_2T_x$ MXenes in Sulfuric Acid

*Ameer Al-Temimy[1,2] *, Kaitlyn Prenger[3], Ronny Golnak[1], Mailis Lounasvuori[1], Michael Naguib[3], Tristan Petit[1] **

[1] Helmholtz-Zentrum Berlin für Materialien und Energie GmbH, Albert-Einstein-Str. 15, 12489 Berlin, Germany
[2] Department of Physics, Freie Universität Berlin, Arnimallee 14, 14195 Berlin, Germany
[3] Department of Physics and Engineering Physics, Tulane University, New Orleans, LA 70118, USA

Keywords: 2D Materials, MXene, cation intercalation, surface chemistry, soft X-ray absorption spectroscopy

Abstract:

Intercalation in $Ti_3C_2T_x$ MXene is essential for a diverse set of applications such as water purification, desalination, electrochemical energy storage and sensing. The interlayer spacing between the $Ti_3C_2T_x$ nanosheets can be controlled by cation intercalation, however, the impact of intercalation on the $Ti_3C_2T_x$ MXene chemical and electronic structures has been poorly investigated so far. Herein, we characterized the electronic structure of pristine, Li-, Na-, K-, and Mg-intercalated $Ti_3C_2T_x$ MXenes dispersed initially in water and 10 mM sulfuric acid (H_2SO_4) using X-ray absorption spectroscopy (XAS). The cation intercalation is found to dramatically influence the chemical environment of Ti atoms. The Ti oxidation of the MXene increases progressively upon intercalation of cations of larger sizes after drying in air, while interestingly a low Ti oxidation is observed for all intercalated MXenes after dispersion in diluted H_2SO_4. *In situ* XAS at the Ti L-edge was conducted during electrochemical oxidation to probe the changes in the Ti oxidation state in the presence of different cations in H_2SO_4 aqueous electrolyte. By applying the sensitivity of the Ti L-edge to probe the oxidation state of Ti atoms, we demonstrate that cation-intercalation and H_2SO_4 environment significantly alter the $Ti_3C_2T_x$ surface chemistry.

1. Introduction

MXenes are a large class of two-dimensional (2D) materials[1,2] that are currently attracting considerable attention due to their exceptional properties for many applications ranging from filtration[3], electrochemical energy storage,[4–8] water purification and desalination,[9–13] to sensing.[14–17] Titanium carbide $Ti_3C_2T_x$ MXenes, a representative member of the large MXene family, is usually terminated by a mixture of –OH, –O–, and –F terminations, denoted by T_x in the following. The O/OH surface terminations of MXene govern the redox mechanism of $Ti_3C_2T_x$ MXenes[18] and are highly hydrophilic which, together with the confined water between MXene sheets, ensures a fast ion diffusion. The redox pseudocapacitance has mostly been studied so far with pristine MXene but the energy density of MXene-based electrodes may be enhanced by intercalation due to the fact that MXene interlayer spacing becomes larger.[7,19] The $Ti_3C_2T_x$ can be intercalated both chemically and electrochemically by mono- and multivalent cations such as Li^+, Na^+, K^+, and Mg^{2+}.[7,20] In general, this variety of cation intercalation was found to have a notable impact on the overall capacitance.[7,21] For water desalination, efficient and reversible electrochemical ion ad/desorption is required.[22] As a result, for practical separation purposes, laminar membranes with horizontally aligned channels constructed from 2D material such as MXene are a perfect choice. Indeed, attractive separation properties of MXene-based membranes demonstrate rejection toward cations of different sizes and charges in solution.[9] Furthermore, a remarkable study shows MXene membranes with highly ordered nanochannel structures can be employed for gas separation such as H_2 purification and CO_2 capture for zero-emission fossil fuel power plant.[23] Ion intercalation in $Ti_3C_2T_x$ MXenes could be used to tune the MXene interlayer spacing and open new possibilities for molecular separation applications using MXene-based membranes.

Cation intercalation is usually characterized using X-ray diffraction (XRD). The XRD measurements have shown that the size of hydrated ions influences the interlayer spacing distance between $Ti_3C_2T_x$ nanosheets (**Figure 1a**).[7,17] The presence of cations between individual MXene sheets does also influence the amount and the structure of the co-intercalated water.[17] As a result, the water mobility is significantly affected by the type, number, and position of the cations within the $Ti_3C_2T_x$ interlayer spacing.[24–26] However, the role of cation intercalation on the surface chemistry of $Ti_3C_2T_x$ MXenes has still been poorly investigated,[27] even though it may strongly impact the oxidation state of Ti atoms and thus the chemical reactivity of the MXene layers.

In this work, the electronic structure of cation-intercalated $Ti_3C_2T_x$ was probed using X-ray absorption spectroscopy (XAS). XAS is an element-specific technique that is very sensitive to surface chemistry and metal oxidation state. In particular, the characterization of transition metal L-edges is very sensitive to the metal chemical environment.[28–30] We have previously applied XAS on $Ti_3C_2T_x$ MXenes intercalated with urea molecules and detected significant changes in the Ti electronic structure.[31] Nevertheless, cations may have a very different mechanism of intercalation between the $Ti_3C_2T_x$ nanosheets due to their smaller size and higher charge, which would affect differently the Ti oxidation state. Furthermore, for electrochemical energy storage applications,

aqueous sulfuric acid electrolyte is mostly used but its impact on the $Ti_3C_2T_x$ MXene surface chemistry remains largely unexplored. In the current study, the electronic structure of $Ti_3C_2T_x$ MXenes after intercalation with Li^+, Na^+, K^+, and Mg^{2+} is characterized by XAS at the Ti L-edge. *Ex situ* XAS measurements were performed to probe the Ti oxidation state of dried cation-intercalated $Ti_3C_2T_x$ initially dispersed in water or sulfuric acid. Furthermore, *in situ* XAS at the Ti L-edge was performed to track the changes in the oxidation of Na-, K-, and Mg-$Ti_3C_2T_x$ in sulfuric acid under anodic potential, leading to the electrochemical oxidation of the $Ti_3C_2T_x$ MXenes. The measurements performed in this study are summarized in **Scheme 1**. The evolution of the oxidation state of Ti atoms in the $Ti_3C_2T_x$ MXenes is significantly affected by cation intercalation and exposure to sulfuric acid and is found to be cation-dependent.

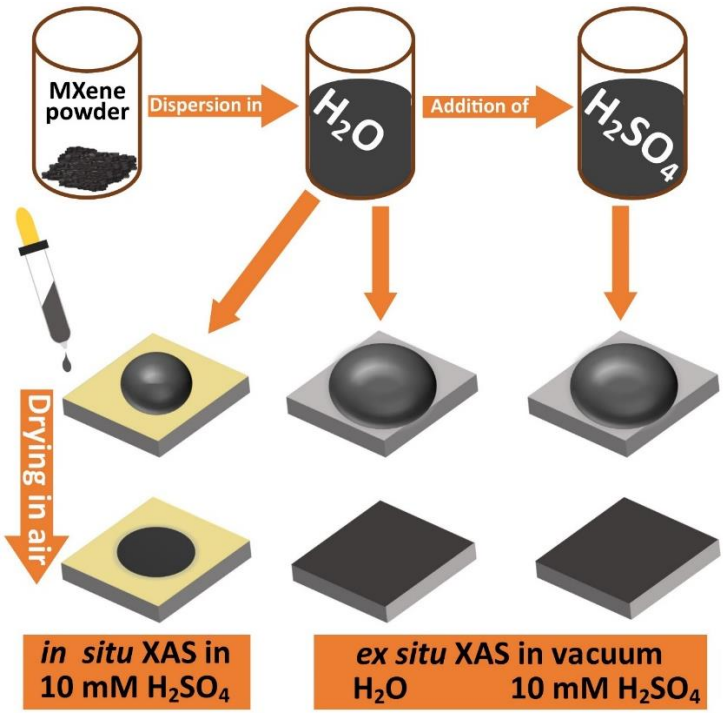

Scheme 1. Schematic of the MXene sample preparation for pristine and cation-intercalated $Ti_3C_2T_x$ films investigated in this work. For *ex situ* and *in situ* XAS, the samples were drop-cast on a conductive silicon substrate and on a gold-coated silicon nitride membrane, respectively. The soft X-ray transparent membrane was then used in an electrochemical flow cell system as shown in **Figure S1**.

2. Results and discussion

2.1. Cation intercalation in $Ti_3C_2T_x$ MXenes

Figure 1a illustrates a schematic of the pristine (top) and cation-intercalated (bottom) $Ti_3C_2T_x$ MXenes. For brevity, the bottom schematic shows the possibility of intercalation by different cations in-between the $Ti_3C_2T_x$ nanosheets. The details of the materials synthesis can be found in the experimental section below. Briefly, the MXenes used in this study were prepared by etching Al from Ti_3AlC_2 using a mixture of HF and LiCl that result in Li-intercalated $Ti_3C_2T_x$, then HCl treatment was conducted to remove Li from in-between the layers to prepare pristine MXene

(labelled $Ti_3C_2T_x$ in the following). Then, this pristine MXene was soaked in different aqueous solutions of LiCl, NaCl, KCl and $MgCl_2$ to form cation-intercalated MXenes: Li-$TI_3C_2T_x$, Na-$Ti_3C_2T_x$, K-$Ti_3C_2T_x$, and Mg-$Ti_3C_2T_x$, respectively. Based on energy-dispersive X-ray spectroscopy (EDS) results, the ratio of Ti to cation in Na-, K-, and Mg-$Ti_3C_2T_x$ MXenes was found to be Ti:Na = 3.00:0.17, Ti:K = 3.00:0.14, and Ti:Mg = 3.00:0.12. It is worth noting that Li cannot be detected using EDS, however, since Li cation is monovalent as Na and K, it is reasonable to assume similar content of Li (0.14-0.17 Li per formula).

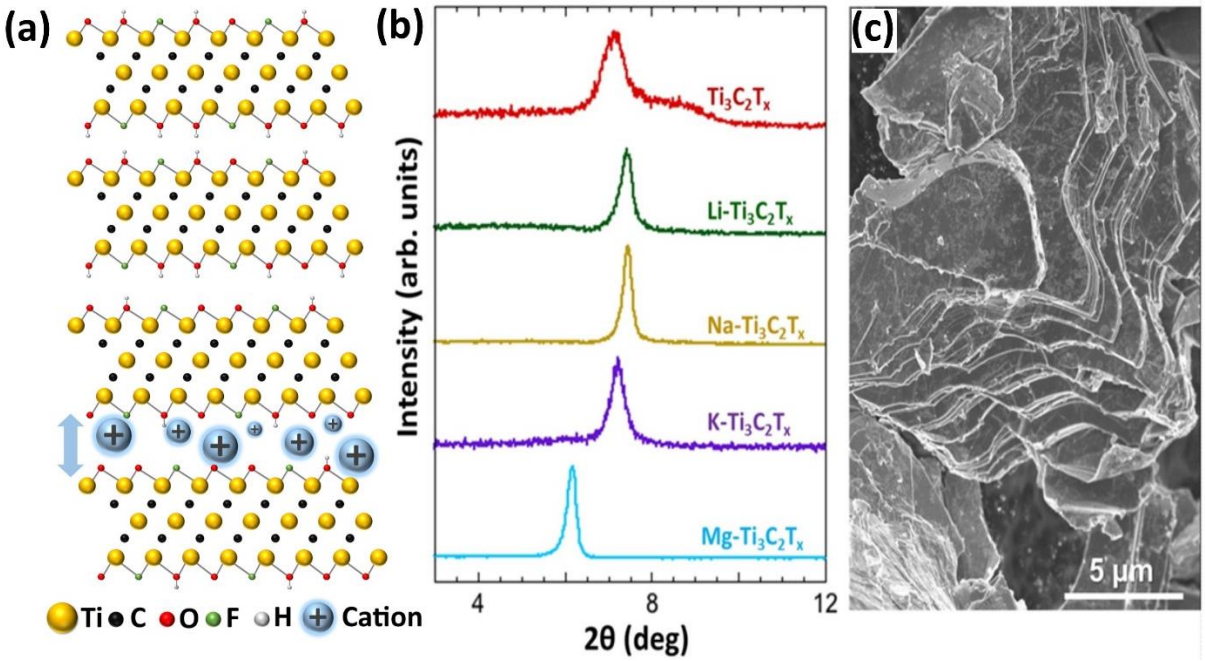

Figure 1 (a) Schematic of pristine $Ti_3C_2T_x$ MXenes (top) and cation-intercalated $Ti_3C_2T_x$ MXenes (bottom) showing the possibility to intercalate $Ti_3C_2T_x$ with cations of different sizes (b) Normalized XRD patterns of pristine, Li-, Na-, K-, and Mg-intercalated $Ti_3C_2T_x$ MXenes. (c) A typical representative SEM image of cation-intercalated $Ti_3C_2T_x$ MXenes (this specific SEM image is Na-MXene for example).

Figure 1b shows normalized XRD (002) peak shifts of the intercalated MXenes studied. Since the position of this peak is inversely related to the *d*-spacing, the position of this peak can be used to compare the relative interlayer spacing of different MXenes. The Li-$Ti_3C_2T_x$, Na-$Ti_3C_2T_x$, and K-$Ti_3C_2T_x$ have a comparable *d*-spacing (with slightly larger spacing for K than Na and Li) but all of them much smaller than that for Mg-$Ti_3C_2T_x$ (see Table S1). This is in agreement with previous reports for cation intercalated MXenes and suggests that the cations remain hydrated after intercalation.[17,20,32] It is worth noting that two peaks can be observed for the pristine MXene suggesting incomplete removal of Li from in-between the layers during the HCl washing step. Another explanation for the two peaks in pristine MXene can be attributed to the co-intercalated water from the washing step in-between the layers for some particles. To check this, the pristine MXene sample was annealed under vacuum at 110 °C for 4h and studied this sample using XRD. Accordingly, we found that the low angle peak vanishes (Figure S4b) suggesting that the co-intercalated water might be responsible for the evolution of this peak. **Figure 1c** shows a scanning

electron microscopy (SEM) image of a typical multilayer MXene used in this study. Here we can clearly see the layered morphology of the MXenes powder.

2.2. *Ex situ* XAS of $Ti_3C_2T_x$ MXenes initially dispersed in water

The electronic structure of intercalated MXene was first characterized *ex situ* using XAS in Total Electron Yield (TEY) mode to observe the influence of intercalation with the different cations. The cation-intercalated MXene samples were allowed to dry in air at room temperature before characterization in vacuum (see **scheme 1**). The XA spectra at the Ti L-edge of $Ti_3C_2T_x$ MXenes comprise two doublets related to the Ti L_3- and L_2-edges, respectively. The Ti L-edge is related to the excitation of Ti $2P_{3/2}$ (L_3-edge) and Ti $2P_{1/2}$ (L_2-edge) core levels to an unoccupied Ti 3d state with 455-462 eV and 462-468 eV excitation energies, respectively. Owing to the ligand field related to binding with oxygen atoms from surface chemical groups, the Ti $L_{3,2}$-edges are each split into two sub peaks corresponding to electronic states with t_{2g} and e_g symmetries. As a result, XAS is highly sensitive to the Ti chemical environment, as illustrated in **Figure 2,** showing the Ti L-edge XA spectra of pristine, Li-, Na-, K-, and Mg-$Ti_3C_2T_x$ MXenes compared to TiO_2 nanoparticles.

While the features of the Ti L-edge XAS are relatively similar for pristine and Li-$Ti_3C_2T_x$ MXenes, they differ significantly for Na-, K-, and Mg- $Ti_3C_2T_x$ MXenes. For pristine (Li-) $Ti_3C_2T_x$ MXenes, the Ti L_3-edge includes a peak at 458.1 (458.3) eV and a shoulder at about 459.8 (460.0) eV corresponding to the t_{2g} and e_g bands, respectively. For larger ions, the Ti L_3 t_{2g} peak at 458.3 eV became sharper and the peak maximum is shifted by +0.2 eV compared to pristine MXene while the pre-edge feature decreases progressively. The Ti L_2-edge shows a broad band with a maximum at 463.6 eV, and a faint shoulder is observed at 465.3 eV for Li- $Ti_3C_2T_x$. Intercalation of $Ti_3C_2T_x$ MXene by Na^+, K^+, and Mg^{2+} cations, on the other hand, results in the splitting of the Ti L_3 edge into well pronounced t_{2g} and e_g sub-bands at 458.3 and 460.0 eV, respectively. Likewise, the Ti L_2 t_{2g} and e_g peaks are well separated at 463.7 and 465.6 eV, respectively. The Ti $L_{3,2}$ t_{2g} and e_g sub-bands become gradually more intense following the order $Li^+ < Na^+ < K^+ < Mg^{2+}$. The e_g band is extremely important due to its high sensitivity to the local environment as the Ti e_g orbitals point directly to the 2p orbitals of the surrounding O atoms.[28,33] The L_2 e_g to t_{2g} peak-to-peak intensity ratio of cation-intercalated $Ti_3C_2T_x$ was 0.83, 0.88, 0.97, and 1.03 for Li, Na-, K-, and Mg-$Ti_3C_2T_x$ MXenes, respectively. In comparison to the TiO_2 nanoparticles with e_g : t_{2g} ratio of 1.25, we can attribute the increase in the e_g component observed for MXene to the higher amount of surface Ti atoms bonded with oxygen in the $Ti_3C_2T_x$ MXenes.

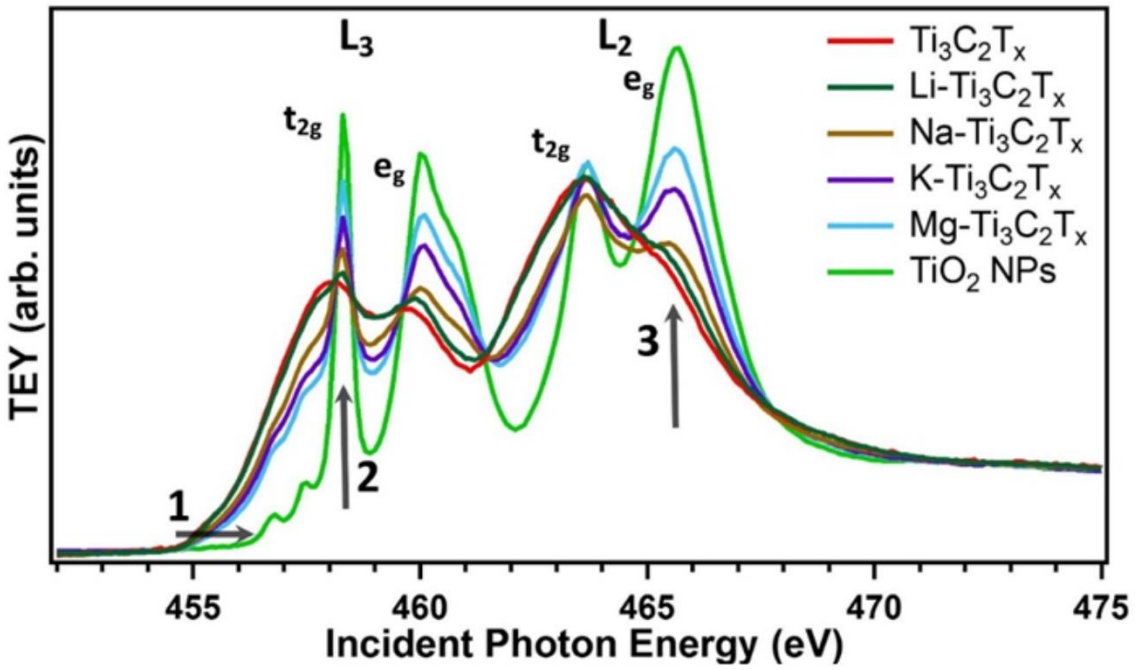

Figure 2. Ti L-edge XA spectra of dried pristine, Li-, Na-, K-, and Mg-intercalated $Ti_3C_2T_x$ MXenes initially dispersed in water compared to TiO_2 nanoparticles. XAS was recorded in total electron yield (TEY) mode in vacuum and the XA spectra are normalized to the TEY signal above 470 eV. The XA spectra reveal three distinctive regions. The feature (1) shows higher Ti oxidation state as the pre-edge region shifts to higher energies. The feature (2) shows a progressive increase in the L_3 t_{2g} peak intensity at the expense of the pre-edge region. The feature (3) reveals a systematic increase in the L_2 e_g peak intensity for larger cations.

The pre-edge region around 455.0-458.0 eV is observed to be relatively more intense for pristine and Li-$Ti_3C_2T_x$ than other intercalated $Ti_3C_2T_x$ MXenes (**Figure 2**). Note that the onset energy position of the Ti L-edge was found empirically to shift to higher energies for higher Ti valence state.[30] Here we used the Ti L-edge onset position to have an estimation of the Ti oxidation state. A prominent pre-edge signal and the presence of the single peak L_2-edge suggest a significant contribution of Ti^{3+} and/or Ti^{2+} species[30] in pristine and Li-$Ti_3C_2T_x$. The shift of the pre-edge onset energy to higher energies along with the evolution of the L_2 e_g to t_{2g} peak-to-peak intensity ratio show an increase in the Ti oxidation state. The latter observation suggests that the oxidation of Ti in pristine and Li-intercalated $Ti_3C_2T_x$ MXenes is close to Ti^{3+} species, whereas the oxidation state of Ti in Na-, K-, and Mg-$Ti_3C_2T_x$ MXenes is gradually closer to Ti^{4+} species. The two low-intensity peaks at 456.8 and 457.5 eV mixed into the L_3 edge observed in Na-, K- and Mg-$Ti_3C_2T_x$ MXenes were previously attributed in TiO_2 materials to the strong interaction between poorly screened 3d electrons and the 2p core hole.[28] The appearance of these peaks confirms the relatively higher Ti oxidation state in Na-, K-, and Mg-$Ti_3C_2T_x$ MXenes after drying in air.

The oxygen bonding was also probed and the XAS at the O K-edge of the cation-intercalated MXene samples are shown in **Figure S2**. In general, the O K-edge of the different MXene samples shows two main features in the energy range between 529 and 535 eV which originate from the transitions between oxygen 1s and 2p states that are hybridized with the empty Ti 3d orbitals.[34]

Furthermore, the O K-edge XA spectra also show a second set of bands in the energy region of about 537-546 eV which can be assigned to the transitions from O 2p states that are hybridized with Ti 4s and 4p states.[34] The XA spectra of pristine, K-, and Mg-$Ti_3C_2T_x$ reveal two features at 531.0 and 533.3 eV (separated by 2.3 eV) assigned to t_{2g} and e_g peaks of the Ti 3d levels, respectively. In Li- and Na-$Ti_3C_2T_x$ MXenes, the maximum of the t_{2g} and e_g features appear at 531.6 and 533.5 eV (separated by 1.9 eV), respectively.

The t_{2g} and e_g peaks at the O K-edge were found to be separated by about 2.5, 2.1, and 1.6 eV for TiO_2, Ti_2O_3, and TiO, respectively.[30] The intensity of the t_{2g} and e_g peaks is directly related to the degree of covalency of the bond between the Ti and O atoms, which becomes stronger with increasing valence state. Therefore, the O K-edge features can provide further information on the geometry of the metal-oxygen bonding.

In Li- and Na-$Ti_3C_2T_x$ MXene samples, the t_{2g} peak maximum is shifted by +0.6 eV relative to other MXene samples. This shift may be caused by the deformation of the hybridization due to the distortion of the local octahedral volume.[35] A similar peak has been reported upon Li^+ or Na^+ ions insertion in TiO_2 materials.[36,37] Previous inelastic neutron scattering (INS) data showed that Li and Na ions are located closer to the $Ti_3C_2T_x$ MXene surface compared to other ions, which may explain why strong distortion of the Ti-O bonds is only observed for these cations.[24] For K and Mg-cations, the increase of the e_g component suggests a higher bonding with oxygen atoms, as previously seen with intercalation of urea molecules.[31]

The XA spectra of pristine and cation-intercalated $Ti_3C_2T_x$ MXenes at the Ti L- and O K-edges demonstrate a profound impact of Li^+, Na^+, K^+, and Mg^{2+} intercalation on the electronic structure of $Ti_3C_2T_x$ MXene. The changes at the Ti L-edge are attributed to a progressive increase in the Ti oxidation state, matching, to a large extent, with larger interlayer distance following the sequence $Li^+ < Na^+ < K^+ < Mg^{2+}$, as shown by the XRD data in **Figure 1b.** The exposure of the cation-intercalated MXene samples to air during the drying process has to be taken into consideration. It is expected that larger interlayer spacing enables the $Ti_3C_2T_x$ surface to be more exposed to water and oxygen from ambient air. The cation size is directly correlated to the interlayer spacing but is not the only factor that influences the Ti oxidation state, otherwise the Ti oxidation state should be relatively close for Li-$Ti_3C_2T_x$ and Mg-$Ti_3C_2T_x$ as the size of Li and Mg ions are comparable. The difference in the Ti oxidation state of Li- and Mg-$Ti_3C_2T_x$ MXene can be attributed to (i) the difference in the cation valency, which might have an impact on the $Ti_3C_2T_x$ MXene electronic distribution, or (ii) the larger cation hydration shell in Mg-intercalated $Ti_3C_2T_x$ MXene samples. It is noteworthy that in a previous study, the hydration shell was found to have a strong impact on the interlayer distance and was found to be cation-dependent.[20]

2.3. *Ex situ* XAS of $Ti_3C_2T_x$ MXenes initially dispersed in sulfuric acid

In a second step, the influence of the sulfuric acid on the Ti electronic structure was investigated. To this aim, the Ti L-edge of pristine, Li-, Na-, K-, and Mg-$Ti_3C_2T_x$ MXenes, initially dispersed

in 10 mM sulfuric acid electrolyte, were characterized in vacuum shortly after drying in air (see **scheme 1**). Significant differences were observed as compared to dried samples initially dispersed in water as can be seen in **Figure 3**. To check if the cations are still intercalated between the MXene nanosheets, we have performed EDS measurements after the treatment with 10 mM H_2SO_4. The EDS data show that the ratio of Ti to cation is 3.00:0.04 for Ti:Na, 3.00:0.08 for Ti:K, and 3.00:0.10 for Ti:Mg. Furthermore, as potassium L-edge lies within the range of the used soft X-ray, the K cations were detected after intercalation as well as after exposure to 10 mM H_2SO_4 (Figure S3). The interlayer spacing distance of all samples investigated increases after exposure to 10 mM H_2SO_4 (Table S1 and Figure S4). This is mostly attributed to co-intercalation of H_3O^+ ions as the difference becomes negligible after annealing at 110°C in vacuum (**Figure S4**). In particular, no significant difference is observed in the pre-edge region between the pristine and the cation-intercalated $Ti_3C_2T_x$ MXenes dispersed in 10 mM H_2SO_4. In pristine, Li-$Ti_3C_2T_x$, and Na-$Ti_3C_2T_x$ the $L_{3,2}$ e_g and t_{2g} have similar profiles which demonstrates a very close oxidation state of the Ti atoms. Interestingly, in K-$Ti_3C_2T_x$ and Mg-$Ti_3C_2T_x$ samples, additional peaks were observed in the $L_{3,2}$ edges at 460.6 and 464.5 eV, respectively. These peaks were previously attributed to distortions typical for Ti in lower valence states than Ti^{4+} species.[30] Furthermore, the L_3 t_{2g} peak maxima of these samples were found to be shifted by +0.5 eV relative to pristine, Li-, and Na-$Ti_3C_2T_x$ MXenes and are comparable to the t_{2g} peak position of TiO_2 nanoparticles (**Figure S5**), whereas a small additional peak appears at 460.6 eV for K- and Mg- $Ti_3C_2T_x$. This suggest that a small amount of oxidized Ti atoms remains on these samples. However, the main Ti oxidation state remains close to that of pristine MXene and the spectral changes are not as intense as for the aqueous dispersions (**Figure 2**).

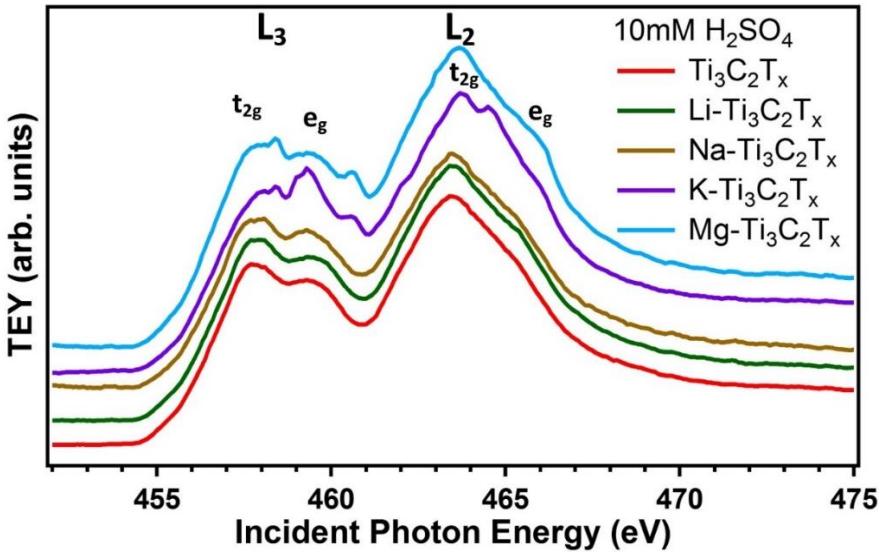

Figure 3. Ti L-edge XA spectra of dried cation-intercalated $Ti_3C_2T_x$ MXene samples initially dispersed in 10 mM sulfuric acid under vacuum conditions. XAS was recorded in the TEY mode and the XA spectra are normalized to the TEY signal above 470 eV.

Likewise, the shoulder at the L_2 e_g position of the K- and Mg-$Ti_3C_2T_x$ is more pronounced compared to other cation-intercalated samples. While Ti oxidation state in Na-$Ti_3C_2T_x$ was found to be between Li-$Ti_3C_2T_x$ and K-$Ti_3C_2T_x$ after dispersion in pure water, its oxidation state after dispersion in diluted H_2SO_4 was similar to the Li-$Ti_3C_2T_x$.

Sulfuric acid has a clear impact on the Ti electronic structure of the different MXene samples. Surprisingly, a relatively low oxidation state is found for all cation-intercalated MXenes compared to MXene initially dispersed in water. The pre-intercalation with sulfuric acid manifests that the $Ti_3C_2T_x$ MXenes are not significantly oxidized after drying in air compared to MXene samples only dispersed in water. This could possibly be related to the higher stability of hydroxylated MXene surface functional groups against oxidation. Storing MXene samples in diluted sulfuric acid may be a promising option for protection of MXene layers against oxidation in water or air, which has been reported in previous reports.[38] In previous studies, lower pH regime was found indeed to impact the surface functional groups as well as observed to enhance the electrochemistry performance.[39,40] This may also relate to the high stability of MXene electrodes in sulfuric acid electrolytes. Further studies will be required to better understand the chemical stability of MXenes in sulfuric acid of different concentrations.

2.4. *In situ* XAS of $Ti_3C_2T_x$ MXenes under applied potential in sulfuric acid

Complementary to *ex situ* characterization, the observation of the $Ti_3C_2T_x$ electronic structure directly in aqueous medium is necessary to understand the impact of cation-intercalation on Ti chemical environment in relevant conditions for application in energy storage or desalination. Especially, in order to better understand the impact of sulfuric acid on the cation-intercalated $Ti_3C_2T_x$ electronic structure, the samples first solvated in water and dried in air were exposed *in situ* to sulfuric acid (see **scheme 1**). In addition, the samples were electrochemically oxidized *in situ* by applying an anodic potential. A high electrochemical potential (+0.6 V *vs* Ag/AgCl) could produce irreversible oxidation of the MXene was chosen, as previously reported by Lorencova *et al* on pristine $Ti_3C_2T_x$ MXene.[41] For potentials below +0.4 V *vs* Ag/AgCl, *Lukatskaya et al.* have shown reversible oxidation of the pristine MXene using *in situ* XAS at the Ti K-edge,[42] which was also confirmed by Raman spectroscopy.[43] *In situ* XAS can be performed in the soft X-ray range using an electrochemical flow cell using partial fluorescence yield (PFY) detection mode.[44] The MXene samples were deposited by drop-casting on a gold-coated 75 nm-thin silicon nitride membrane that is used to separate the liquid from the vacuum chamber and enables soft X-ray transmission.

Figure 4 shows the Ti L-edge spectral features of different cation-$Ti_3C_2T_x$ MXenes in 10 mM H_2SO_4 electrolyte at open potential and +0.6 V vs. Ag/AgCl. The relatively low H_2SO_4 concentration was chosen to avoid etching of the thin Au layer used as current collector in the electrochemical flow cell (see **Figure S1**). **Figure 4a** presents the spectral features of Ti L-edge upon introducing the H_2SO_4 to Na-, K-, and Mg-$Ti_3C_2T_x$ samples at open circuit potential. The 10 mM H_2SO_4 aqueous environment results in different XA spectra features between Na-, K-, and

Mg-$Ti_3C_2T_x$ samples compared to their dried counterpart measured under vacuum conditions. In general, after introducing the 10 mM H_2SO_4, the Ti oxidation state was found to be the lowest in Na-$Ti_3C_2T_x$ followed by Mg- and K-$Ti_3C_2T_x$ MXenes. This estimation is based on the onset energy position and the Ti L_3 t_{2g} peak sharpness. In contrast to the Na-$Ti_3C_2T_x$, the Ti oxidation state of Mg- and K-$Ti_3C_2T_x$ MXenes was observed to be relatively higher compared to the dried samples initially dispersed in 10 mM H_2SO_4 measured under vacuum conditions. Thereafter, we monitored the Ti L-edge at +0.6 V applied potential vs. Ag/AgCl (**Figure 4b-d**).

Figure 4b demonstrates the electrochemical oxidation of the Na-$Ti_3C_2T_x$ MXene sample. The pre-edge onset energy position shifts to higher energies after applying a positive voltage (**Figure S7**). This shift confirms a significant increase in the average oxidation state of the Ti atoms at anodic potential. Additionally, irrespective of the changes associated with the onset energy position: (i) the t_{2g} peak was found to be at 458.5 eV which corresponds to 0.2 eV shift to higher energies compared to dried sample dispersed in water or XAS detection mode of the peak might become broader in H_2SO_4 aqueous environment. (ii) The L_2 t_{2g}-e_g splitting is unequivocally missing relative to the dried sample dispersed in pure water and resembles the trend observed in the dried sample initially dispersed in 10 mM H_2SO_4.

Unlike Na-$Ti_3C_2T_x$ MXene, the electrochemical oxidation of K-$Ti_3C_2T_x$ shown in **Figure 4c** does not express a relative shift in the onset energy position at positive 0.6 V applied potential (**Figure S8**). Relative to the dried spectrum of K-$Ti_3C_2T_x$ initially dispersed in water, the L_3 t_{2g} peak becomes more intense and the L_2 t_{2g}-e_g splitting was found to be preserved. It has to be mentioned that the t_{2g} peak was also shifted by 0.2 eV to higher energies relative to the dried sample initially dispersed in water following the tendency observed in the sample initially dispersed in H_2SO_4. Likewise, the Ti L-edge of the Mg-$Ti_3C_2T_x$ MXene shown in **Figure 4d** reveals a contribution from the Ti^{4+} species as validated by the intense and sharp t_{2g} peak. The intensity and the sharpness of the t_{2g} peak relative to the pre-edge feature was observed to be more pronounced at +0.6 V applied potential, indicating a higher Ti oxidation state (**Figure S9**). At the same time, the pre-edge onset is shifted to higher energies, which indicates a higher oxidation at +0.6 V bias voltage, the t_{2g} peak itself was found to be much more intense.

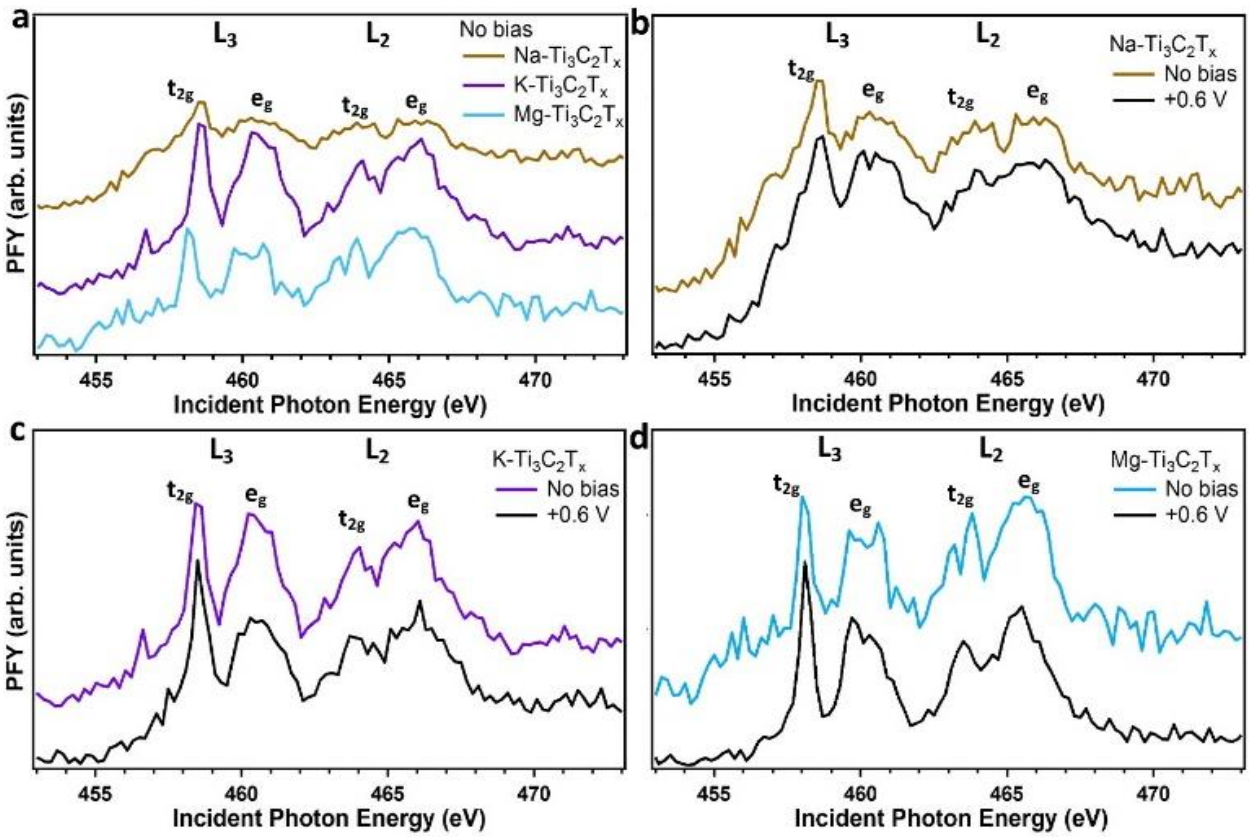

Figure 4. *In situ* Ti L-edge XA spectra of different cation-intercalated $Ti_3C_2T_x$ MXenes in 10 mM H_2SO_4 and applied potentials vs. Ag/AgCl. (a) after introducing the sulfuric acid to different cation-intercalated $Ti_3C_2T_x$ MXenes at open circuit potential. (b) Na-$Ti_3C_2T_x$. (c), K-$Ti_3C_2T_x$. (d), Mg-$Ti_3C_2T_x$. The spectrum in black in (b), (c), and (d) corresponds to +0.6 V applied potential. XA spectra were recorded in partial fluorescence yield (PFY) using an electrochemical flow cell.

The cation intercalation and the interaction with sulfuric acid were found to play a significant role in the final oxidation state of Ti atoms. In Na-$Ti_3C_2T_x$ sample, a relatively low Ti oxidation was observed, most likely due to the fact that Na^+ is located relatively closer to the surface of the MXene sheets compared to K and Mg cations. A clear oxidation of the Ti is then observed at +0.6 V vs. Ag/AgCl.

On the other hand, for K- and Mg-$Ti_3C_2T_x$ samples, the XA spectra recorded at open circuit potential show that the surface Ti atoms were already quite oxidized. This demonstrate that initial oxidation in air, as shown in Figure 2, is irreversible even after exposure to 10 mM H_2SO_4. The Ti surface atoms can only be reduced if they are exposed to 10 mM H_2SO_4 before drying in air (**Figure 3**). As a result, the impact of electrochemical oxidation is less visible than for Na- $Ti_3C_2T_x$, which is also confirmed by the smaller current flowing through the K- and Mg- $Ti_3C_2T_x$ samples during *in situ* measurements at +0.6V (**Figure S6**). In K-$Ti_3C_2T_x$, no clear shift in the Ti L-edge onset energy position was induced by the positive 0.6 V bias voltage. Nevertheless, the L_3 t_{2g} was found to be enhanced relative to the e_g peak which may indicate a slightly higher Ti oxidation state. For Mg-$Ti_3C_2T_x$, the anodic potential in H_2SO_4 has a slight impact on the Ti electronic structure as the pre-edge onset energy position shifts to higher energies and the L_3 t_{2g} also increases, as shown in

Figure 4d. As the interlayer spacing is the largest for Mg-$Ti_3C_2T_x$ (**Figure 1b**), the Ti atoms are thus relatively more vulnerable to oxidation.

3. Conclusion

In this study, we investigated the effect of cation-intercalation with Li^+, Na^+, K^+, and Mg^{2+} on the MXene electronic structure using XAS at the Ti L-edge in various environments. After dispersion in water and drying in air, the oxidation state of Ti atoms in $Ti_3C_2T_x$ MXenes is dramatically altered by cation intercalation and is found to progressively increase with larger cations. On the other hand, after dispersion in 10 mM H_2SO_4, the Ti atoms remain largely unaffected by cation-intercalation and have a similar chemical environment than pristine $Ti_3C_2T_x$ MXenes. This suggests that exposure of MXene to a small amount of H_2SO_4 aqueous solution may protect the MXene surface from oxidation. Finally, the impact of *in situ* exposure to 10 mM H_2SO_4 and to the application of anodic electrochemical potentials on the Ti oxidation state was also investigated. *In situ* XAS measurements of Na-, K- and Mg-$Ti_3C_2T_x$ MXenes demonstrated an increase in the average Ti oxidation state upon electrochemical oxidation (+0.6 V vs Ag/AgCl). This work illustrates that the chemical sensitivity of Ti L-edge XAS may open new chemical insights into cation intercalation and MXene surface oxidation mechanisms. As the oxidation state plays a significant role in electrochemical performance of $Ti_3C_2T_x$ MXenes, this sensitivity could also be applied to probe electrochemical energy storage and conversion processes on MXenes.

4. Experimental section

Materials:

MAX Ti_3AlC_2 was synthesized as reported by Huang and Mochalin.[45] Powders of titanium (Alfa Aesar, -325 mesh), aluminum (Alfa Aesar -325 mesh), and graphite (Alfa Aesar, APS 7-15 micron) were mixed in atomic ratio of 3.00:1.10:1.88 in a Turbula T2F mixer for 3 h using zirconia balls, then the powders were furnaced in a tube furnace under flowing argon at 1600°C for 2 h with a heating rate of 10°C/minute. Cation-intercalated $Ti_3C_2T_x$ samples were produced similarly to Ghidiu et al.[20] Ti_3AlC_2 powder was ground to -325 mesh and slowly added to a solution of lithium chloride in 10%wt hydrofluoric acid (HF) in ratios of 1g of Ti_3AlC_2 to 10ml of etchant, with 1:5 molar ratio of Ti_3AlC_2 to LiCl. The etching was carried out at room temperature with stirring for 24 h. This was followed by washing with excess deionized water until a pH >6 was reached. The still wet powders were soaked in 37% HCl (30mL per every 1 g powder), centrifuged, and supernatant was discarded. This step was repeated for a total of 5 cycles of acid washing. The powders were again washed with excess deionized water until a pH > 6 was reached. Despite the several washing steps, some Li cations may remain intercalated. The wet powders were divided into 5 equal portions, and one portion was soaked in 1M LiCl, 1M NaCl, 1M KCl, 0.5M $MgCl_2$, or deionized water (40mL solution for each gram of powder) for 1 h, after which the solutions were centrifuged, and supernatants discarded. This was followed by repeating the soaking of the wet powders in fresh solutions, listed above, for 24 h. Then, the mixtures were washed with deionized water 3 times, discarding supernatants at each step. Finally, the intercalated powders of

Li-, Na-, K-, and Mg-$Ti_3C_2T_x$ MXenes and pristine $Ti_3C_2T_x$ were dried by vacuum assisted filtration.

X-ray Diffraction: X-ray diffraction patterns of cation-intercalated and pristine $Ti_3C_2T_x$ were obtained using a Rigaku DMAX 2200 Cu K_α x-ray diffractometer. The scans were conducted with a step size of 0.02° and a 1°/second dwell time from 3°-65° 2θ. SEM images were taken using a Hitachi 4800 High-Resolution SEM. To confirm full etching and cation intercalation, energy dispersive x-ray spectroscopy was performed on a Hitachi 3400 scanning electron microscope with Oxford Inca software.

Ex situ XAS measurements in vacuum environment: The samples in both *ex situ* studies were characterized by XAS using Total Electron Yield (TEY) detection mode with the LiXEdrom endstation at the U49-2_PGM1 beamline of the synchrotron light source BESSY II operated by HZB. MXene samples were deposited by drop-casted on conductive Si substrates and dried in air for about three hours to obtain the dried samples of $Ti_3C_2T_x$, Li-$Ti_3C_2T_x$, Na-$Ti_3C_2T_x$, K-$Ti_3C_2T_x$, and Mg-$Ti_3C_2T_x$ MXenes as well as a thin TiO_2 NPs film. The different cation-intercalated MXene powders were dispersed in Milli-Q water and sonicated for 90 minutes. For the *ex situ* study of MXenes initially dispersed in water, the sonicated different cation-intercalated MXene powders were centrifuged at 3500 rpm for 15 minutes and further sonicated for several minutes in order to obtain a homogeneous suspension (ink-like) before deposition by drop-casting. The 10 mM H_2SO_4 was then added to the resultant suspension followed by a short sonication for several minutes in order to get the final colloidal used for the *ex situ* study of MXene samples initially dispersed in sulfuric acid. Anatase TiO_2 nanoparticles (PL-TiO, Plasmachem, GmbH), used as reference for Ti L-edge XAS, had an average particle size of 4-8 nm and were stabilized by a 10 wt.% nitric acid (HNO_3) solution. The Ti L-edge XA spectra were normalized to the background signal before (455 eV) and after (470 eV) the edge features.

***In situ XAS measurements in liquid environment*:** Experiments were conducted at the U49-2_PGM1 undulator beamline of BESSY II using the LiXEdrom endstation. A membrane-based electrochemical flow cell[44] enabled us to perform *in situ* XAS measurements using Partial Fluorescence Yield (PFY) mode. The Si_3N_4 membranes (produced by Silson) had a window size of 1.0 mm x 0.5 mm used to isolate the liquid environment from the vacuum chamber (10^{-6} mbar range), which is required for soft XAS measurements. The window area is composed of a 75 nm-thick Si_3N_4 membrane coated with 5 nm Cr (adhesive layer) and 10 nm Au. The MXene samples (initially dispersed in water, same samples as in the *ex situ* study) were deposited by drop-casted on the Au coated membrane and dried under air. The electrochemical reaction was conducted in a three-electrode system using an Ag/AgCl reference electrode (Innovative Instruments, Inc.) and a Pt counter electrode (Goodfellow, GmbH). Initial measurements using 1M H_2SO_4 have shown rapid degradation of the gold current collector under applied potential, which was not the case with 10 mM H_2SO_4. This relatively low H_2SO_4 concentration was therefore chosen for this study. Each

in situ XA spectrum is the average summation of four to six spectra measured at different positions of the X-ray transparent window (see Figure S10 for XA spectra including error bars).

The liquid flow in the electrochemical membrane-based flow cell is controlled by a Legato 270 syringe pump (KD Scientific Inc.) and operated in push-pull mode with a flow rate of 1 mL/min to ensure a constant flow of the electrolyte during the experiments, which enables efficient sulfuric acid renewal during measurement.

AUTHOR INFORMATION

Corresponding Author

 Email: ameer.al-temimy@helmholtz-berlin.de and tristan.petit@helmholtz-berlin.de

Author Contributions

The manuscript was written by A.A. with contributions from all coauthors. A.A. designed and conducted the *ex situ* studies with experimental support from R.G. and M.L. A.A. and T.P. designed and conducted the *in situ* electrochemical XAS measurements. A.A. performed the entire XAS data analysis. M.N. and K.P. conducted the material synthesis and the full characterization. M.N. and T.P. supervised the research.

Supporting Information. XAS at the O K-edge and K L-edge, XRD pattern after dispersion in H_2SO_4 and after drying in air, further details on XAS at the Ti L-edge, in situ chronoamperometry.

ACKNOWLEDGMENT

A.A. acknowledges the German Academic Exchange Service (DAAD) for financial support during the PhD. A.A. and T.P. acknowledge the financial support from the Volkswagen Foundation (Freigeist Fellowship No. 89592). A.A. is grateful for additional funding support by HZB, Prof. Simone Raoux, and the DAAD devoted to a short term research stay at Tulane University, New Orleans, USA. MAX and intercalated MXenes synthesis and characterization at Tulane University was supported as part of the Fluid Interface Reactions, Structures and Transport (FIRST) Center, an Energy Frontier Research Center funded by the U.S. Department of Energy, Office of Science, Office of Basic Energy Sciences. We acknowledge Dr. Babak Anasori support with some of the sample preparation. The authors acknowledge the kind support by staff members of the BESSY II synchrotron facility especially the beamline scientists at the beamline U49-2_PGM1. We thank HZB for the allocation of synchrotron radiation beamtime. A. A. is grateful to the research visit opportunity awarded by the Fulbright visiting scholars program in Iraq to the US where a remarkable scientific collaboration was initiated with Prof. Michael Naguib to provide some of the necessary samples for the PhD project of A. A. in Germany.

REFERENCES

(1) Naguib, M.; Mashtalir, O.; Carle, J.; Presser, V.; Lu, J.; Hultman, L.; Gogotsi, Y.; Barsoum, M. W. Two-Dimensional Transition Metal Carbides. *ACS Nano* **2012**, *6* (2), 1322–1331.

(2) Naguib, M.; Mochalin, V. N.; Barsoum, M. W.; Gogotsi, Y. 25th Anniversary Article: MXenes: A New Family of Two-Dimensional Materials. *Adv. Mater.* **2014**, *26* (7), 992–1005.

(3) Peng, Q.; Guo, J.; Zhang, Q.; Xiang, J.; Liu, B.; Zhou, A.; Liu, R.; Tian, Y. Unique Lead Adsorption Behavior of Activated Hydroxyl Group in Two-Dimensional Titanium Carbide. *J. Am. Chem. Soc.* **2014**, *136* (11), 4113–4116.

(4) Anasori, B.; Lukatskaya, M. R.; Gogotsi, Y. 2D Metal Carbides and Nitrides (MXenes) for Energy Storage. *Nature Reviews Materials*. 17, 2017, p 16098.

(5) Naguib, M.; Come, J.; Dyatkin, B.; Presser, V.; Taberna, P. L.; Simon, P.; Barsoum, M. W.; Gogotsi, Y. MXene: A Promising Transition Metal Carbide Anode for Lithium-Ion Batteries. *Electrochem. commun.* **2012**, *16* (1), 61–64.

(6) Lukatskaya, M. R.; Kota, S.; Lin, Z.; Zhao, M. Q.; Shpigel, N.; Levi, M. D.; Halim, J.; Taberna, P. L.; Barsoum, M. W.; Simon, P.; et al. Ultra-High-Rate Pseudocapacitive Energy Storage in Two-Dimensional Transition Metal Carbides. *Nat. Energy* **2017**, *6*.

(7) Lukatskaya, M. R.; Mashtalir, O.; Ren, C. E.; Dall'Agnese, Y.; Rozier, P.; Taberna, P. L.; Naguib, M.; Simon, P.; Barsoum, M. W.; Gogotsi, Y. Cation Intercalation and High Volumetric Capacitance of Two-Dimensional Titanium Carbide. *Science* **2013**, *341* (6153), 1502–1505.

(8) Eames, C.; Islam, M. S. Ion Intercalation into Two-Dimensional Transition-Metal Carbides: Global Screening for New High-Capacity Battery Materials. *J. Am. Chem. Soc.* **2014**, *136* (46), 16270–16276.

(9) Ren, C. E.; Hatzell, K. B.; Alhabeb, M.; Ling, Z.; Mahmoud, K. A.; Gogotsi, Y. Charge- and Size-Selective Ion Sieving Through $Ti_3C_2T_x$ MXene Membranes. *J. Phys. Chem. Lett.* **2015**, *6* (20), 4026–4031.

(10) Ding, L.; Wei, Y.; Wang, Y.; Chen, H.; Caro, J.; Wang, H. A Two-Dimensional Lamellar Membrane: MXene Nanosheet Stacks. *Angew. Chemie - Int. Ed.* **2017**, *56* (7), 1825–1829.

(11) Kang, K. M.; Kim, D. W.; Ren, C. E.; Cho, K. M.; Kim, S. J.; Choi, J. H.; Nam, Y. T.; Gogotsi, Y.; Jung, H. T. Selective Molecular Separation on $Ti_3C_2T_x$-Graphene Oxide Membranes during Pressure-Driven Filtration: Comparison with Graphene Oxide and MXenes. *ACS Appl. Mater. Interfaces* **2017**, *9* (51), 44687–44694.

(12) Wang, J.; Chen, P.; Shi, B.; Guo, W.; Jaroniec, M.; Qiao, S. Z. A Regularly Channeled Lamellar Membrane for Unparalleled Water and Organics Permeation. *Angew. Chemie - Int. Ed.* **2018**, *57* (23), 6814–6818.

(13) Hong, S.; Ming, F.; Shi, Y.; Li, R.; Kim, I. S.; Tang, C. Y.; Alshareef, H. N.; Wang, P. Two-Dimensional $Ti_3C_2T_x$ MXene Membranes as Nanofluidic Osmotic Power Generators. *ACS Nano* **2019**, *13* (8), 8917–8925.

(14) Kim, S. J.; Koh, H. J.; Ren, C. E.; Kwon, O.; Maleski, K.; Cho, S. Y.; Anasori, B.; Kim, C. K.; Choi, Y. K.; Kim, J.; et al. Metallic $Ti_3C_2T_x$ MXene Gas Sensors with Ultrahigh Signal-to-Noise Ratio. *ACS Nano* **2018**, *12* (2), 986–993.

(15) Lee, E.; Vahidmohammadi, A.; Prorok, B. C.; Yoon, Y. S.; Beidaghi, M.; Kim, D. J. Room Temperature Gas Sensing of Two-Dimensional Titanium Carbide (MXene). *ACS Appl. Mater. Interfaces* **2017**, *9* (42), 37184–37190.

(16) Muckley, E. S.; Naguib, M.; Ivanov, I. N. Multi-Modal, Ultrasensitive, Wide-Range Humidity Sensing with Ti_3C_2 Film. *Nanoscale* **2018**, *10* (46), 21689–21695.

(17) Muckley, E. S.; Naguib, M.; Wang, H. W.; Vlcek, L.; Osti, N. C.; Sacci, R. L.; Sang, X.; Unocic, R. R.; Xie, Y.; Tyagi, M.; et al. Multimodality of Structural, Electrical, and Gravimetric Responses of Intercalated MXenes to Water. *ACS Nano* **2017**, *11* (11), 11118–11126.

(18) Zhan, C.; Naguib, M.; Lukatskaya, M.; Kent, P. R. C.; Gogotsi, Y.; Jiang, D. E. Understanding the MXene Pseudocapacitance. *J. Phys. Chem. Lett.* **2018**, *9* (6), 1223–1228.

(19) Gao, Q.; Come, J.; Naguib, M.; Jesse, S.; Gogotsi, Y.; Balke, N. Synergetic Effects of K^+ and Mg^{2+} Ion Intercalation on the Electrochemical and Actuation Properties of the Two-Dimensional Ti_3C_2 MXene. *Faraday Discuss.* **2017**, *199*, 393–403.

(20) Ghidiu, M.; Halim, J.; Kota, S.; Bish, D.; Gogotsi, Y.; Barsoum, M. W. Ion-Exchange and Cation Solvation Reactions in Ti3C2 MXene. *Chem. Mater.* **2016**, *28* (10), 3507–3514.

(21) Mashtalir, O.; Lukatskaya, M. R.; Zhao, M. Q.; Barsoum, M. W.; Gogotsi, Y. Amine-Assisted Delamination of Nb_2C MXene for Li-Ion Energy Storage Devices. *Adv. Mater.* **2015**, *27* (23), 3501–3506.

(22) Su, X.; Kushima, A.; Halliday, C.; Zhou, J.; Li, J.; Hatton, T. A. Electrochemically-Mediated Selective Capture of Heavy Metal Chromium and Arsenic Oxyanions from Water. *Nat. Commun.* **2018**, *9* (1), 4701.

(23) Ding, L.; Wei, Y.; Li, L.; Zhang, T.; Wang, H.; Xue, J.; Ding, L. X.; Wang, S.; Caro, J.; Gogotsi, Y. MXene Molecular Sieving Membranes for Highly Efficient Gas Separation. *Nat. Commun.* **2018**, *9* (1).

(24) Osti, N. C.; Naguib, M.; Ganeshan, K.; Shin, Y. K.; Ostadhossein, A.; Van Duin, A. C. T.; Cheng, Y.; Daemen, L. L.; Gogotsi, Y.; Mamontov, E.; et al. Influence of Metal Ions Intercalation on the Vibrational Dynamics of Water Confined between MXene Layers. *Phys. Rev. Mater.* **2017**, *1* (6), 065406.

(25) Osti, N. C.; Naguib, M.; Ostadhossein, A.; Xie, Y.; Kent, P. R. C.; Dyatkin, B.; Rother, G.; Heller, W. T.; Van Duin, A. C. T.; Gogotsi, Y.; et al. Effect of Metal Ion Intercalation on the Structure of MXene and Water Dynamics on Its Internal Surfaces. *ACS Appl. Mater. Interfaces* **2016**, *8* (14), 8859–8863.

(26) Shpigel, N.; Levi, M. D.; Sigalov, S.; Mathis, T. S.; Gogotsi, Y.; Aurbach, D. Direct Assessment of Nanoconfined Water in 2D Ti 3 C 2 Electrode Interspaces by a Surface Acoustic Technique. *J. Am. Chem. Soc.* **2018**, *140* (28), 8910–8917.

(27) Xie, Y.; Naguib, M.; Mochalin, V. N.; Barsoum, M. W.; Gogotsi, Y.; Yu, X.; Nam, K. W.; Yang, X. Q.; Kolesnikov, A. I.; Kent, P. R. C. Role of Surface Structure on Li-Ion Energy Storage Capacity of Two-Dimensional Transition-Metal Carbides. *J. Am. Chem. Soc.* **2014**, *136* (17), 6385–6394.

(28) Kucheyev, S. O.; Van Buuren, T.; Baumann, T. F.; Satcher, J. H.; Willey, T. M.; Meulenberg, R. W.; Felter, T. E.; Poco, J. F.; Gammon, S. A.; Terminello, L. J. Electronic Structure of Titania Aerogels from Soft X-Ray Absorption Spectroscopy. *Phys. Rev. B - Condens. Matter Mater. Phys.* **2004**, *69* (24), 245102.

(29) Petit, T.; Ren, J.; Choudhury, S.; Golnak, R.; Lalithambika, S. S. N.; Tesch, M. F.; Xiao, J.; Aziz, E. F. X-Ray Absorption Spectroscopy of TiO_2 Nanoparticles in Water Using a Holey Membrane-Based Flow Cell. *Adv. Mater. Interfaces* **2017**, *4* (23), 1700755.

(30) Stoyanov, E.; Langenhorst, F.; Steinle-Neumann, G. The Effect of Valence State and Site Geometry on Ti $L_{3,2}$ and O K Electron Energy-Loss Spectra of Ti_xO_y Phases. *Am. Mineral.* **2007**, *92* (4), 577–586.

(31) Al-Temimy, A.; Anasori, B.; Mazzio, K. A.; Kronast, F.; Seredych, M.; Kurra, N.; Mawass, M.-A.; Raoux, S.; Gogotsi, Y.; Petit, T. Enhancement of Ti_3C_2 MXene Pseudocapacitance After Urea Intercalation Studied by Soft X-Ray Absorption Spectroscopy. *J. Phys. Chem. C* **2020**, acs.jpcc.9b11766.

(32) Célérier, S.; Hurand, S.; Garnero, C.; Morisset, S.; Benchakar, M.; Habrioux, A.; Chartier, P.; Mauchamp, V.; Findling, N.; Lanson, B.; et al. Hydration of $Ti_3C_2T_x$ MXene: An Interstratification Process with Major Implications on Physical Properties. *Chem. Mater.* **2019**, *31* (2), 454–461.

(33) Hsu, M.-Y.; Yang, W.-C.; Teng, H.; Leu, J. Microstructure and Composition of TiO[Sub 2] Nanotube Arrays Fabricated with HF and NH_4F Electrolytes and Their Evolution during Annealing. *J. Electrochem. Soc.* **2011**, *158* (3), K81.

(34) De Groot, F. M. F.; Grioni, M.; Fuggle, J. C.; Ghijsen, J.; Sawatzky, G. A.; Petersen, H. Oxygen 1s X-Ray-Absorption Edges of Transition-Metal Oxides. *Phys. Rev. B* **1989**, *40* (8), 5715–5723.

(35) De Groot, F. M. F.; Faber, J.; Michiels, J. J. M.; Czyyk, M. T.; Abbate, M.; Fuggle, J. C. Oxygen 1s X-Ray Absorption of Tetravalent Titanium Oxides: A Comparison with Single-Particle Calculations. *Phys. Rev. B* **1993**, *48* (4), 2074–2080.

(36) Okumura, T.; Fukutsuka, T.; Yanagihara, A.; Orikasa, Y.; Arai, H.; Ogumi, Z.; Uchimoto, Y. Electronic and Local Structural Changes with Lithium-Ion Insertion in TiO_2-B: X-Ray Absorption Spectroscopy Study. *J. Mater. Chem.* **2011**, *21* (39), 15369–15377.

(37) Liu, Y.; Zhao, F.; Li, J.; Li, Y.; McLeod, J. A.; Liu, L. Influence of Crystal Phase on TiO_2 Nanowire Anodes in Sodium Ion Batteries. *J. Mater. Chem. A* **2017**, *5* (37), 20005–20013.

(38) Zhang, C. J.; Pinilla, S.; McEvoy, N.; Cullen, C. P.; Anasori, B.; Long, E.; Park, S. H.; Seral-Ascaso, A.; Shmeliov, A.; Krishnan, D.; et al. Oxidation Stability of Colloidal Two-Dimensional Titanium Carbides (MXenes). *Chem. Mater.* **2017**, *29* (11), 4848–4856.

(39) Natu, V.; Sokol, M.; Verger, L.; Barsoum, M. W. Effect of Edge Charges on Stability and

Aggregation of $Ti_3C_2T_z$ MXene Colloidal Suspensions. *J. Phys. Chem. C* **2018**, *122* (48), 27745–27753.

(40) Natu, V.; Clites, M.; Pomerantseva, E.; Barsoum, M. W. Mesoporous MXene Powders Synthesized by Acid Induced Crumpling and Their Use as Na-Ion Battery Anodes. *Mater. Res. Lett.* **2018**, *6* (4), 230–235.

(41) Lorencova, L.; Bertok, T.; Dosekova, E.; Holazova, A.; Paprckova, D.; Vikartovska, A.; Sasinkova, V.; Filip, J.; Kasak, P.; Jerigova, M.; et al. Electrochemical Performance of $Ti_3C_2T_x$ MXene in Aqueous Media: Towards Ultrasensitive H_2O_2 Sensing. *Electrochim. Acta* **2017**, *235*, 471–479.

(42) Lukatskaya, M. R.; Bak, S. M.; Yu, X.; Yang, X. Q.; Barsoum, M. W.; Gogotsi, Y. Probing the Mechanism of High Capacitance in 2D Titanium Carbide Using in Situ X-Ray Absorption Spectroscopy. *Adv. Energy Mater.* **2015**, *5* (15).

(43) Hu, M.; Li, Z.; Hu, T.; Zhu, S.; Zhang, C.; Wang, X. High-Capacitance Mechanism for $Ti_3C_2T_x$ MXene by in Situ Electrochemical Raman Spectroscopy Investigation. *ACS Nano* **2016**, *10* (12), 11344–11350.

(44) Schwanke, C.; Golnak, R.; Xiao, J.; Lange, K. M. Electrochemical Flowcell for In-Situ Investigations by Soft x-Ray Absorption and Emission Spectroscopy. *Rev. Sci. Instrum.* **2014**, *85* (10), 103120.

(45) Huang, S.; Mochalin, V. N. Hydrolysis of 2D Transition-Metal Carbides (MXenes) in Colloidal Solutions. *Inorg. Chem.* **2019**, *58* (3), 1958–1966.

Table of content graphic: